Vertically Oriented Ti–Pd Mixed Oxynitride Nanotube Arrays for Enhanced Photoelectrochemical Water Splitting

Nageh K. Allam,[†,*] Adam J. Poncheri,[‡] and Mostafa A. El-Sayed[‡,*]

[†]Department of Electrical Engineering and Computer Science, Massachusetts Institute of Technology, Cambridge, Massachusetts 02139, United States and [‡]Laser Dynamics Laboratory, School of Chemistry and Biochemistry, Georgia Institute of Technology, Atlanta, Georgia 30332-0400, United States

ABSTRACT In recent years, considerable efforts have been made to design and discover photoactive nanostructured materials that can be used as anodes in water photoelectrolysis cells. Herein, we report on the growth of a novel photoanode material composed of self-ordered, vertically oriented nanotube arrays of titanium–palladium mixed oxynitride films *via* anodization of Ti–Pd alloy in an electrolyte solution of formamide containing NH_4F at room temperature, followed by annealing in an ammonia atmosphere. The nanostructure topology was found to depend on both the anodization time and the applied voltage. Our results demonstrate the ability to grow mixed oxynitride nanotube array films that are several micrometers thick. The Ti–Pd oxynitride nanotube array films were utilized in solar-spectrum water photoelectrolysis, demonstrating a photocurrent density of 1.9 mA/cm^2 and a ~5-fold increase in the photoconversion efficiency under AM 1.5 illumination (100 mW/cm^2, 1.0 M KOH) compared to pure TiO_2 nanotubes fabricated and tested under the same conditions. The obtained efficiency is among the highest reported values for a TiO_2 nanotube-based photoelectrochemical cell. This enhancement in the photoconversion efficiency is related to the synergistic effects of Pd alloying, nitrogen doping, and the unique structural properties of the fabricated nanotube arrays.

KEYWORDS: anodization · Ti–Pd–O–N · oxynitride nanotubes · photocurrent · water splitting

Green and efficient energy technologies are the driving force of a paradigm shift based on how we should power our society. Nanoscience will play a decisive role in the transformation from fossil fuels to renewable sources.[1,2] Toward this end, the utilization of solar energy as a renewable source is the most attractive and convenient option to pursue.[1,2] It is now generally recognized that nanoscale control of metal oxide architectures leads to the development of new materials and systems with unique physical and chemical properties.[3] In this regard, the anodization technique is considered to be an efficient and well-developed process for the growth of a variety of nanoarchitectures.[4–10] As an important n-type semiconductor material, due to its low cost, stability, and vectorial charge transfer, anodically fabricated TiO_2 nanotube arrays have recently stimulated increasing attention because of their promising applications in fields such as solar hydrogen generation by water photoelectrolysis.[9,11] However, the poor spectral response of the material as well as its relatively low efficiency of light utilization, due to its wide band gap (3.0–3.2 eV), limits its efficient use for solar energy harvesting.[11] More efficient visible light harvesting would render this material quite attractive for solar energy conversion. A very active approach to this problem is doping the material with appropriate anions and cations to render this oxide sensitive to visible light.[9] Although doping has been demonstrated as an efficient approach to introduce visible light absorption to TiO_2, the currently used doping protocols are not without serious problems. Structural artifacts/defects introduce defect-dopant–lattice interactions that can mask the fundamental interactions of the dopant with the lattice.[9,12] The decoration of TiO_2 nanotubes with metal and/or semiconductor nanoparticles is another approach that has been used to improve the spectral response and catalytic properties of the material.[13–16] However, the lack to achieve control over the nanoparticles such as their particle size, cleanness, and distribution on the nanotubes' surfaces/walls and the possibility of nanoparticles to aggregate limit their efficient use. The distribution of particles can be better controlled with the introduction of linker molecules that attach nanoparticles to the nanotube surface, but this presents more complicated charge carrier recombination problems.[17,18] A recent and promising approach to overcome the above-mentioned

* Address correspondence to melsayed@gatech.edu, nkallam@mit.edu.

Received for review March 25, 2011 and accepted May 10, 2011.

Published online May 13, 2011
10.1021/nn201136t

limitations, as they pertain to photocatalytic properties and applications, is to develop, optimize, and employ semiconductor materials with 1D nanoarchitectures of mixed oxides. In a recent work, Mor and co-workers reported the anodization of Ti−Fe films to fabricate Ti−Fe−O mixed oxide nanotube arrays with enhanced photoelectrochemical water splitting performance.[19] On the basis of those promising results, they expanded the work to fabricate a p-type Ti−Cu−O nanoarchitectured electrode through the anodization of Ti−Cu films and used it to construct a self-biased photodiode for water splitting.[20] Kusama and co-workers reported a combinatorial approach to systematically investigate the visible light response of Fe−Ti−M (M: various metal elements) oxides for photoelectrochemical water splitting.[21] Among the 25 elements tested, the Fe−Ti−Sr mixed oxide has been identified as the best combination because it gave the highest photocurrent. Allam and co-workers were able to grow a uniform suite of Ti−Nb−Zr−O mixed oxide nanotube arrays.[22] The fabricated mixed oxide nanotubes showed a ~17.5% increase in the photoelectrochemical water oxidation efficiency as compared to pure TiO_2 nanotubes of comparable length. Nitrides and oxynitrides are another class of materials that are widely used as photocatalysts for water splitting under visible light irradiation.[23] Vitiello and co-workers reported the fabrication of titanium oxynitride nanotube arrays by Ti anodization followed by nitridation in NH_3.[24] The resulting oxynitride nanotubes showed significant visible light response and enhanced photoelectrochemical properties. Ferrero and co-workers reported the nanostructured titanium oxynitride mesoporous thin films to be efficient visible-light-active photocatalysts due to the discrete introduction of N, which caused a shift of the titania absorption edge.[25] Additionally, Kim and co-workers reported the anodization of the Ti−N substrates for the purpose of fabricating Ti−O−N nanotubes, which also showed high photoresponse in the visible range of the solar spectrum.[26]

On the basis of the above survey, it seems logical that the best way to fabricate highly efficient photoanodes may be to combine both approaches simultaneously, that is, doping (through alloying) and nitriding (to get oxynitrides). To the best of our knowledge, there is no published work on the growth and use of anodically fabricated *mixed* oxynitrides of titania nanotube arrays for water photoelectrolysis. We note that some work was reported regarding the combination of metal nanoparticle decoration and nitriding, which showed enhanced photocatalytic properties.[27−29] However, the same problems of nanoparticle assembly, load, distribution, and artifacts are still present. Herein, we fabricate Ti−Pd mixed oxynitride nanotube arrays *via* anodization of Ti−Pd alloy in fluoride-ion-containing electrolyte followed by nitridation to convert the anodically fabricated nanotubes into oxynitrides. This system was chosen for the following reasons:

1. Pd-containing catalysts are well-known for their considerable photocatalytic activity.[27−33] Also, Pd oxide has a band gap energy in the visible region (0.8−2.2 eV depending on crystalinity and purity) and thus has been widely used as a modifier to enhance light absorption and conductivity of wide band gap semiconductors.[34,35]
2. The use of an alloy as a starting substrate will ensure the homogeneous distribution of Pd in the fabricated nanotubes matrix overcoming the problems seen upon the decoration of TiO_2 nanotubes with metal nanoparticles as detailed above.
3. Oxynitrides have narrower band gaps than the corresponding metal oxides because the metal−nitrogen bond in oxynitrides has a potential energy higher than that of the metal−oxygen bond in metal oxides. Moreover, oxynitrides are known for their stability against anodic dissolution in alkaline media, making them ideal candidates for water photolysis applications.[27]

Our ability to fabricate nanotubular structure of Ti−Pd mixed oxynitrides is significant because the nanotube array architecture allows for the precise design and control of the geometrical features, which allows one to achieve a material with specific light absorption and propagation characteristics.[9] Also, the aligned porosity, crystallinity, and oriented nature of the nanotubular structure make this architecture an attractive electron percolation pathway for vectorial charge transfer between interfaces.[36,37] The fabricated Ti−Pd mixed oxynitride nanotube arrays showed one of the highest photoconversion efficiencies when employed in a photoelectrochemical water splitting system. We hope that this study will open new avenues of research for the exploration of additional combinations of materials and various new applications.

RESULTS AND DISCUSSION

Morphological and Structural Characterization. We aimed at anodizing pure titanium and Ti−Pd alloy samples in formamide-based electrolytes because the anodization of titanium[9] and its alloys[19,20,22] in aqueous electrolytes usually results in the formation of short nanotubes with irregular outer diameters that contain ridges and circumferential serrations. This organic solvent is well-known for the anodization of titanium and results in the formation of smooth nanotubes several micrometers in length. This morphology is achieved by reducing the changes in pH and suppresses the local concentration fluctuations during the anodization process.[9] Figure 1 shows the top-view FESEM images obtained for Ti−Pd samples anodized in formamide-based electrolytes containing 0.2 M NH_4F, 0.1 M H_3PO_4,

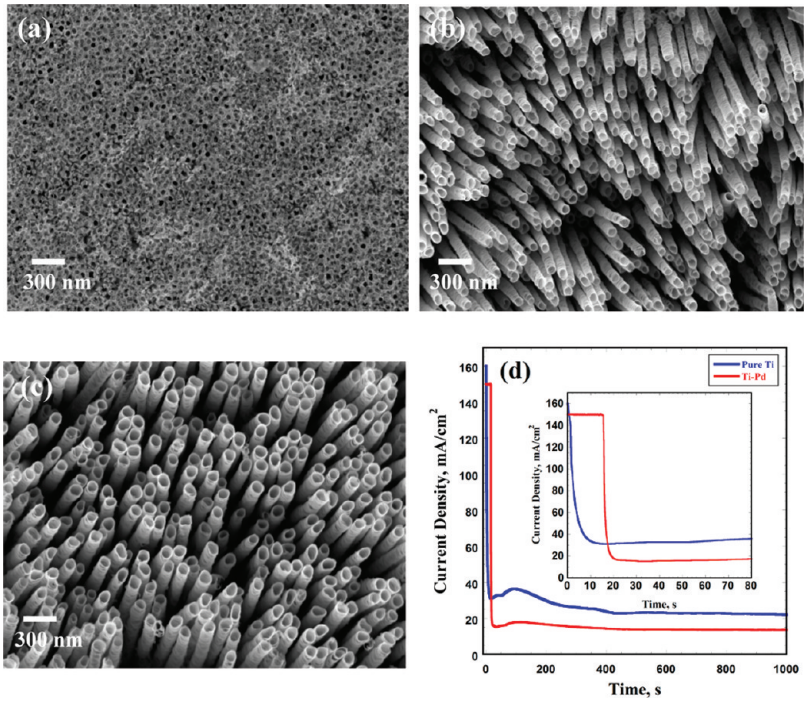

Figure 1. FESEM top-view images for Ti−Pd samples anodized in formamide electrolytes containing 0.2 M NH_4F and 0.1 M H_3PO_4 at 20 V for (a) 5 h, (b) 15 h, and (c) 24 h; (d) corresponding current−time relations for Ti and Ti−Pd samples anodized at 20 V.

and 3 vol % H_2O at 20 V for different time intervals (5, 15, and 24 h). Note that only porous structure is obtained for the sample anodized for 5 h (Figure 1a). The pore diameter in the case of Ti−Pd (45 ± 5 nm) was found to be smaller than that obtained upon anodizing pure Ti (70 ± 5 nm) under the same conditions. Increasing the anodization time to 15 h resulted in the formation of vertically oriented nanotube arrays ~3 μm long with outer diameters of 130 ± 4 nm and wall thicknesses of 17 ± 2 nm (Figure 1b). Extending the anodization time to 24 h resulted in the formation of ~6 μm long self-organized, vertically oriented Ti−Pd nanotube arrays with almost the same outer diameter and wall thickness (Figure 1c). However, anodization for 36 h resulted in the formation of a thick debris layer redeposited on top of the nanotubes (see Supporting Information, Figure S1) preventing them from being effectively used. An attempt to remove the debris layer through ultrasonication resulted in the collapse of the thin-walled tubes and/or causing them to peel off the alloy substrate. Generally, it seems that anodizing Ti alloys results in the formation of nanotubes with thinner wall thicknesses than pure Ti.[19,20,22]

The current−time relations recorded during the anodization of pure Ti and Ti−Pd samples at 20 V for 24 h are shown in Figure 1d. The plots are typical compared to those previously reported for Ti metal anodized in similar electrolytes.[9] Note that the current curve in the case of Ti−Pd starts with an incubation period where the current remains constant for ~20 s followed by a sharp decrease. Also, the current density in the case of Ti−Pd is lower than that of pure Ti, indicating that Ti−Pd is more resistant to etching than pure Ti. The nanotube formation mechanism is described in detail in the literature.[9,38] Briefly, the first step involves the anodic oxidation of the alloy substrate through its interaction with oxygen ions (O^{2-}) in the electrolyte, resulting in the formation of a poorly conducting thin oxide layer that is responsible for the sudden drop in the measured current (Figure 1d). It is believed that the nanotubular structure formation includes a competition between electrochemical etching and chemical dissolution processes,[9] where small pits are initially formed, due to the localized dissolution of the previously formed thin oxide layer, followed by the coalescence of these pits to form pores leading to the observed slight increase in current with time. Upon increasing the anodization time, pores become deeper and wider with small inner-tube void diameters and relatively thick tube walls that continue to grow until well-organized nanotube arrays are formed. It is important to mention that the nanotube growth should stop once the rates of electrochemical etching and the chemical dissolution become equal.[9]

As the fabricated nanotube arrays are usually amorphous, we annealed them in either oxygen or NH_3 environments to crystallize and convert them into oxynitrides. The reaction between NH_3 and TiO_2 was explained elsewhere[38] based on the five-coordinated Ti^{4+} surface sites (Lewis acid) acting as the

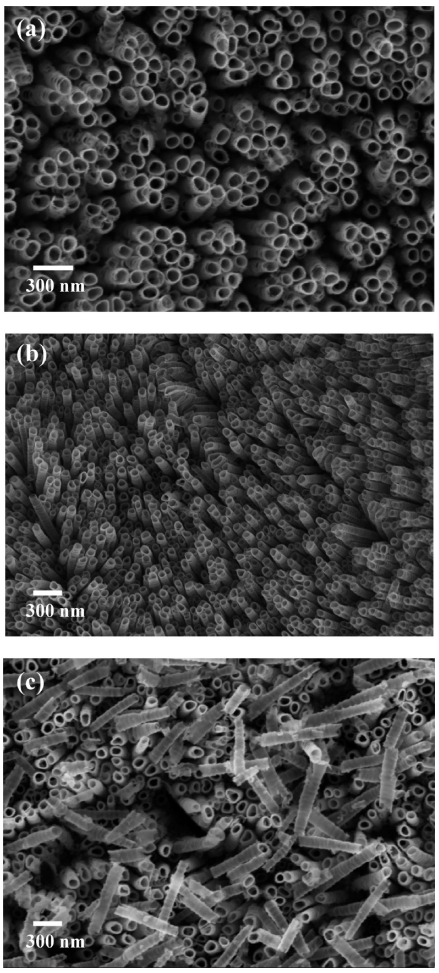

Figure 2. FESEM top-view images of Ti−Pd nanotube array samples annealed at (a) 550 °C in oxygen, (b) 550 °C in NH_3, and (c) 600 °C in NH_3.

reaction center for anchoring NH_3 and for its subsequent chemical transformation into oxynitride. Figure 2 shows the top-view FESEM images for Ti−Pd nanotube arrays annealed at 550 °C for 5 h in dry oxygen atmosphere (Figure 2a) and in NH_3 atmosphere (Figure 2b). Note that the nanotubular structure is preserved in both cases. Upon annealing at higher temperatures (>550 °C) in either oxygen or NH_3, the structure begins to collapse. Figure 2c shows the Ti−Pd nanotube array sample annealed at 600 °C in an NH_3 atmosphere. As noted earlier, nanotube collapse is made evident by broken parts peeled from scattered areas of the substrate.

X-ray photoelectron spectroscopy (XPS) is considered to be the most convenient method for the distinction between oxides and oxynitride because both oxides and oxynitride have virtually overlapping X-ray diffraction patterns.[39,40] Figure 3 shows the XPS results from a Ti−Pd sample that was anodized in a formamide-based electrolyte containing 0.2 M NH_4F, 0.1 M H_3PO_4, and 3 vol % H_2O at 20 V for 24 h. Figure 3a shows Ti 2p spectra where two peaks were obtained, which correspond to Ti $2p_{3/2}$ and Ti $2p_{1/2}$ photoemission spectra. The O 1s peak (Figure 3b) consists of a symmetric singlet at ~530.4 eV, characteristic of lattice oxygen for metal oxides.[22] Another singlet was observed at 402.3 eV and can be attributed to N 1s (Figure 3c). Varghese and coworkers observed a similar peak during anodization of pure titanium using similar electrolytes.[41] They related this peak to the incorporation of nitrogen into the nano tubes,[41] while others related this peak to chemisorbed nitrogen.[42] A high-resolution scan over Pd (Figure 3d) shows the existence of two peaks which can be assigned to Pd $3d_{3/2}$ (340.5 eV) and Pd $3d_{5/2}$ (335.4 eV) with the peak appearing at 335.4 eV indicating the presence of Pd^{2+}.[43] Annealing the sample at 400 °C in NH_3 does not result in any change in the photoemission peaks of Ti 3d, O 1s, and Pd 3d. However, the N 1s photoemission spectra become broader and can be deconvoluted into two peaks at 398.9 and 400.7 eV that could be assigned to characteristic energy losses[44] or might be due to adsorbed NH_x species[45] (see Figure S2 in Supporting Information). Annealing at 500 °C resulted in similar results compared to those obtained at 400 °C but with an additional broad peak in the N 1s spectra appearing at 395−397 eV, which indicates the possibility of nitrogen doping[46] (see Figure S3). Increasing the annealing temperature to 550 °C resulted in a profound change in the photoemission spectra of the material. Figure 4 shows the emission spectra for Ti 3d, O 1s, N 1s, and Pd 3d. Note that the peaks of Ti 3d (Figure 4a) are shifted to lower binding energies (458.2 and 464.1 eV) as compared to those of the unannealed sample (458.5 and 464.3 eV), which indicates an increased electron cloud density around Ti. This can be related to the introduction of a less electronegative atom into the crystal lattice of TiO_2. This finding supports the introduction of N because it has a smaller electronegativity (3.04 on Pauling scale) compared to O (3.44 on Pauling scale). Note that the Ti $2p_{3/2}$ photoemission line at 458.5 eV is diagnostic for oxynitride (Ti−O−N).[47] This assignment is consistent with the spectra of O 1s photoelectrons (Figure 4b) composed of two peaks appearing at 530.2 and 531.8 eV and are characteristic of Ti oxide and Ti oxynitride, respectively.[42] Note also that the photoemission line for N 1s (Figure 4c) appears at 397.4 eV, confirming the formation of oxynitride.[42] The spectrum for Pd 3d (Figure 4d) does not show a profound change compared to the as-anodized sample (Figure 3d). The photoemission line at 337.6 eV becomes broader with a shoulder appearing at ~334.1 eV, indicating the possible existence of Pd^0 along with Pd^{2+} (337.6 eV) in the TiO_2 film. Wu and co-workers observed a similar shoulder for Pd^0 in their Pd-doped TiO_2 thin films.[48] On the basis of these results, it seems that the nanotubular structure is exceptionally reactive toward nitridation, producing oxynitrides

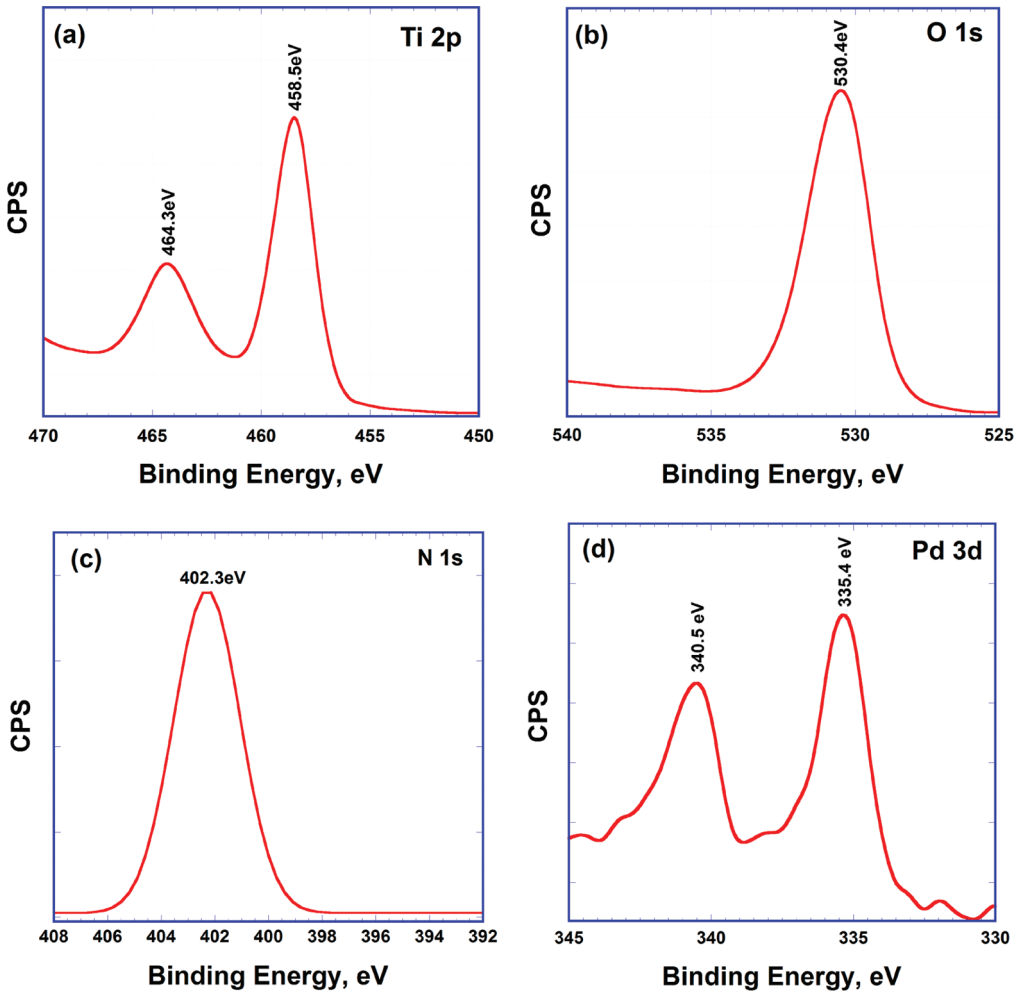

Figure 3. XPS spectra obtained for as-anodized Ti−Pd nanotubes fabricated by the anodization of Ti−Pd alloy in a formamide electrolyte containing 0.2 M NH_4F and 0.1 M H_3PO_4 at 20 V for 24 h; see text.

when annealed in an ammonia atmosphere at 550 °C. Note that titania powders[49] and porous films[50] were shown to be unreactive with ammonia at temperatures below 600 °C.

Photoelectrochemical Water Oxidation Properties. A preliminary (proof-of-concept) photoelectrochemical activity test for water photoelectrolysis using the synthesized Ti−Pd nanotube arrays was carried out. Figure 5a shows the photocurrent density *versus* potential in 1.0 M KOH solution under AM 1.5G (100 mW/cm^2) illumination for TiO_2 (annealed at 550 °C in oxygen), Ti−Pd (annealed at 550 °C in oxygen), and Ti−Pd (annealed at 500 and 550 °C in NH_3) nanotube array electrodes. Note that both the nanotube length (~6 μm long) and annealing time (5 h) were kept constant for all samples. The photocurrent of the Ti−Pd nanotube sample annealed in oxygen is slightly higher than that of the pure TiO_2 nanotube sample. However, a drastic increase in photocurrent was observed for Ti−Pd nanotube arrays annealed in NH_3 with an additional photocurrent increase when changing the annealing temperature from 500 to 550 °C. The dark current was less than 5 μA/cm^2 for all samples tested over the displayed potential range. The open-circuit voltage (V_{OC}) presented by the onset potential in the photocurrent−voltage curve, corresponding to the difference between the apparent Fermi level of the working and reference electrodes,[11] is −0.894 V for the Ti−Pd nanotubes annealed at 550 °C in NH_3. This value is more negative than that of TiO_2 (−0.813 V) and Ti−Pd (−0.884 V) nanotubes annealed at the same temperature in an oxygen atmosphere, demonstrating a shift in the Fermi level to more negative potential.[11] With respect to water splitting, this open-circuit voltage represents the contribution of light toward the minimum voltage needed for water splitting potential (~1.23 V).[11] The current−voltage characteristics of an illuminated semiconductor electrode in contact with a redox electrolyte can be described using the following equation:[36]

$$i = i_{ph} - i_0\left[\exp\left(\frac{e_0 V}{kT}\right) - 1\right] \quad (1)$$

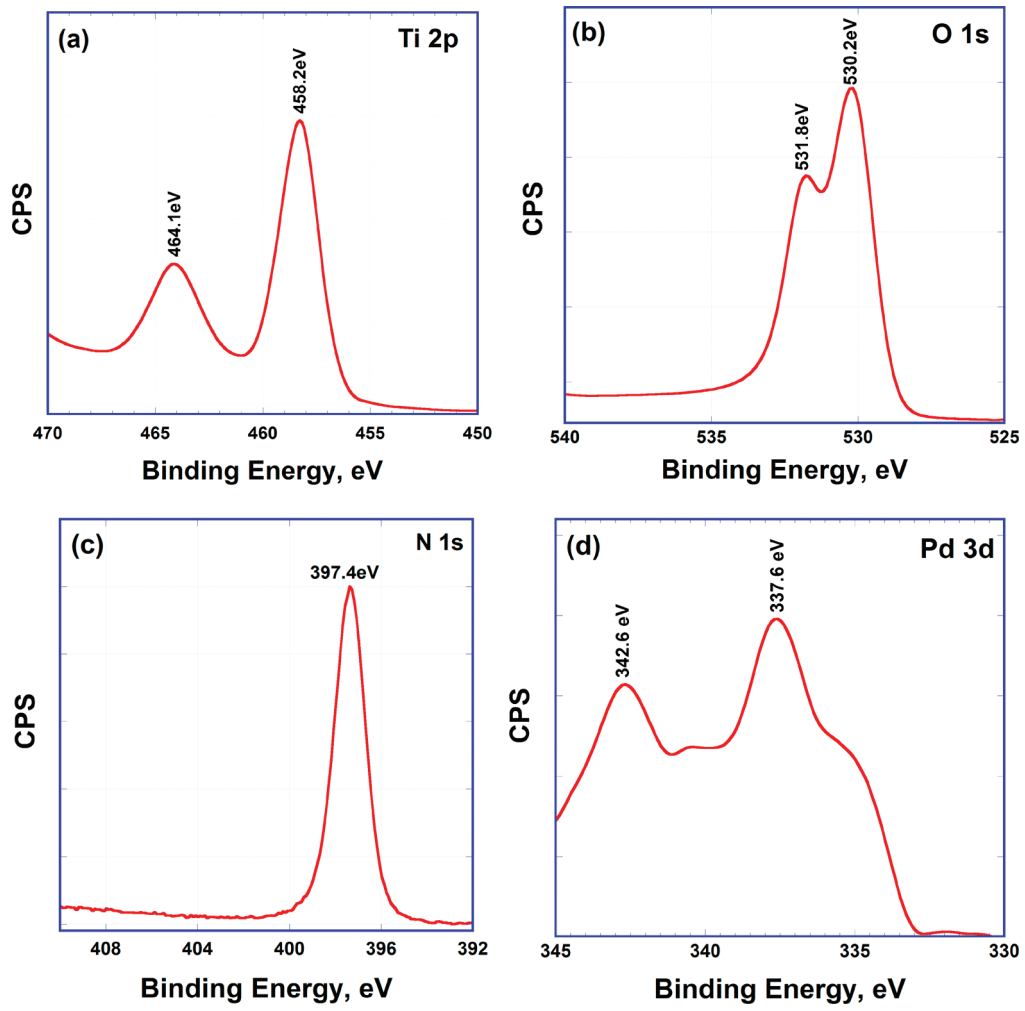

Figure 4. XPS spectra obtained for Ti−Pd nanotube arrays annealed at 550 °C in NH_3 atmosphere for 5 h; see text.

where i is the net current obtained by adding the majority and minority current components, i_0 is the reverse bias saturation current, and i_{ph} is the illumination current which is proportional to the photon flux. All tested nanotube array electrodes show n-type behavior, that is, positive photocurrents at anodic potentials. This is in agreement with literature that states doping TiO_2 with up to 8.4% Pd will not change its n-type behavior.[51] For this type of semiconductor, the surface electron density (N_s) decreases with the applied anodic potentials (E_a) as[22]

$$N_s = N_b \exp\left[-e\left(\frac{E_a - V_{fb}}{kT}\right)\right] \quad (2)$$

where N_b is the bulk electron density in the semiconductor, V_{fb} is its flat-band potential, e is the elementary charge, k is Boltzmann's constant, and T is the absolute temperature. Note that $N_s < N_b$ for an n-type semiconductor at all potentials positive of V_{fb}.

For crystalline semiconductors, provided that their absorption coefficient is not too high, the potential dependence of the squared photocurrent (i^2_{ph}) was shown to follow the following relation:[22,36]

$$i^2_{ph} = \left(\frac{2\varepsilon\varepsilon_0 I^2 \alpha}{N}\right)(E_a - V_{fb}) \quad (3)$$

where α is the absorption coefficient, N is the effective density of states, E_a is the applied potential, and V_{fb} is the flat-band potential. Figure 5b shows the squared photocurrent as a function of applied voltage. The current gradually increases, becoming linear with applied bias, indicating that the photogenerated charges are being efficiently separated by the electric field of the depletion layer.[22] At higher potentials, the squared photocurrent−potential plot slightly deviates from linearity due to saturation resulting from the near complete collection of photogenerated charge carriers and is in agreement with literature concerning TiO_2 photoanodes.[11,22] Using linear regression, the linear part of Figure 5b was fitted to eq 3 to estimate the V_{fb} for the tested electrodes.[22] It was found that the V_{fb} of Ti−Pd nanotubes annealed in NH_3 (−0.967 V) is slightly more negative than that of Ti−Pd nanotubes annealed

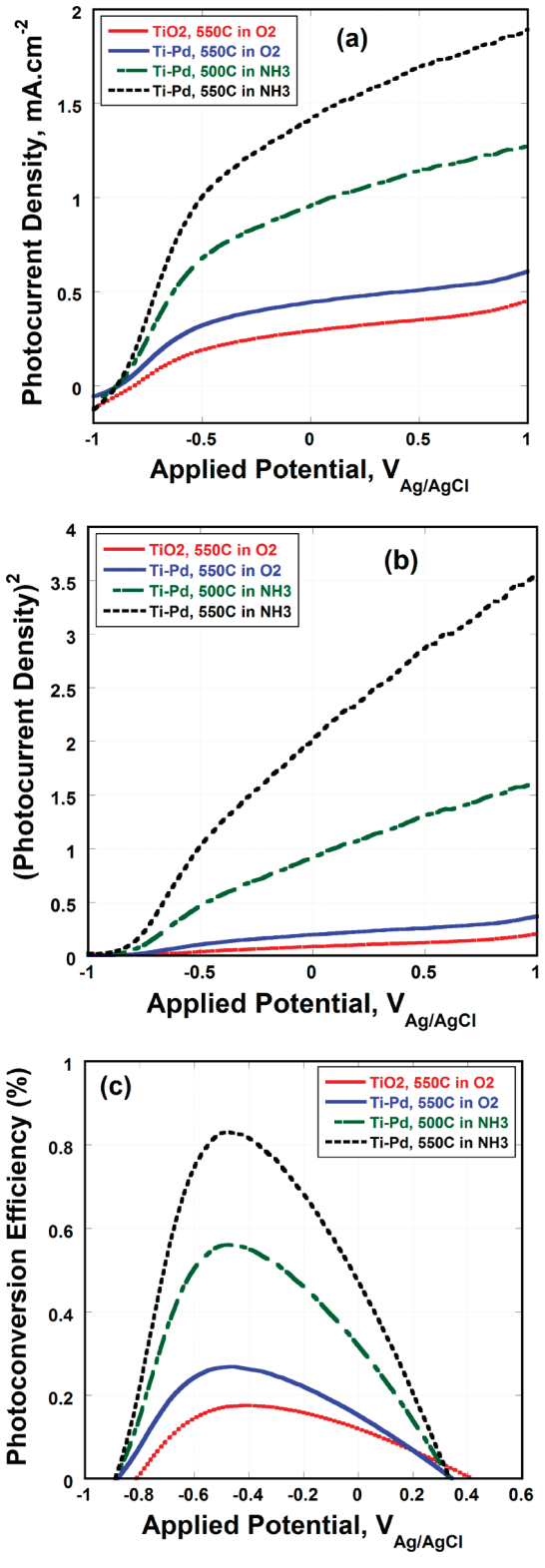

Figure 5. (a) Photocurrent density *vs* potential in 1 M KOH solution under AM 1.5G illumination (100 mW/cm^2) for pure TiO_2 and Ti−Pd nanotube electrodes, (b,c) corresponding squared photocurrent density *vs* potential and the photoconversion efficiency, respectively .

in an oxygen atmosphere (−0.963 V), which is in turn more negative than that of pure TiO_2 (−0.960 V), which is in parallel with the V_{OC} trend.

The corresponding light energy to chemical energy conversion (photoconversion) efficiencies are shown in Figure 5c. The photoconversion efficiency η was calculated *via*[11]

$$\eta\% = [(\text{total power output} - \text{electrical power input})/\text{light power input}] \times 100 = j_p[(E^0_{rev} - |E_{appl}|)/I_0] \times 100 \quad (4)$$

where j_p is the photocurrent density (mA/cm^2), $J_pE^0_{rev}$ is the total power output, $j_p|E_{appl}|$ the electrical power input, and I_0 is the power density of incident light (mW/cm^2). E^0_{rev} is the standard reversible potential, which is 1.23 V_{NHE}, and the applied potential $E_{appl} = E_{meas} - E_{aoc}$, where E_{meas} is electrode potential (*versus* Ag/AgCl) of the working electrode at which photocurrent was measured under illumination and E_{aoc} is the electrode potential (*versus* Ag/AgCl) of the same working electrode at open-circuit conditions under the same illumination and in the same electrolyte. The photoconversion efficiencies for the synthesized nanotube arrays, under AM 1.5G illumination, are ≈0.18, 0.27, and 0.83% for the TiO_2, Ti−Pd−O, and Ti−Pd−O−N nanotubes having the same length (∼6 μm). The reported AM 1.5 photoconversion efficiency, so far, for TiO_2 nanotube-based photoelectrochemical cells is 0.6% or slightly higher.[52] In our case, the maximum efficiency was found to be 0.83%, which is about 38% higher than any efficiency reported thus far. Note that increasing the annealing temperature (in NH_3 atmosphere) from 500 to 550 °C resulted in increasing the photoconversion efficiency from 0.56 to 0.83%. However, increasing the annealing temperature to 600 °C resulted in a serious collapse of the tubular structure, and hence the sample was not tested. Also, it was shown that annealing porous TiO_2 films and powders at 600 °C in NH_3 promotes the formation of larger amounts of oxygen vacancies and consequently resulted in lower photocatalytic activity.[50] It was reported that increasing the photocatalytic activity of N-doped titania materials under visible light is due to the formation of localized N 2p states that exist as discrete levels above the valence band, suggesting that nitrogen addition occurs as a substitutionally or interstitially bound nitrogen species.[46] Both nitrogen doping (sample annealed at 500 °C in NH_3) and the formation of oxynitride (sample annealed at 550 °C in NH_3) led to a significant enhancement in the light harvesting capability of the material (see Figure S4 in Supporting Information). The N-doped sample showed a shift in the absorption edge up to 442 nm with an absorption tail extending all the way to 700 nm. Varghese and co-workers reported that nitrogen doping of TiO_2 nanotubes led to the formation of N 2p states above the titania VB that shifts the absorption edge of titania to 540 nm.[41] The oxynitride sample showed even better shift in the absorption edge to 577 nm with

an extended tail up to 700 nm, as well. Assuming the applicability of the relation

$$E = \frac{1240}{\lambda} \quad (5)$$

where E is the band gap of the material and λ is the corresponding absorption edge wavelength, one can estimate the band gap values as 2.8 and 2.15 eV for the samples annealed in NH_3 atmosphere at 500 and 550 °C, respectively. This change in band gap can be used to explain the observed enhancement in the photoconversion efficiency. On the other hand, the enhanced photoresponse of the Ti−Pd oxynitride nanotube samples can be related to the distinct tube structure and composition. For example, the presence of Pd contributes to the enhanced photoactivity of the material as Pd oxide has a band gap that is located within the visible region of the light spectrum.[51] Also, the thin wall thickness of our synthesized Ti−Pd oxynitride nanotube arrays is expected to play a vital role in such an enhanced photoresponse.[11] The nanotubular architecture, with a wall thickness of 17 ± 2 nm, ensures that the photogenerated holes are never generated far from the semiconductor−electrolyte interface.[11] The half-value of the wall thickness is significantly less than the minority carrier diffusion length (~20 nm in TiO_2),[9,22] ensuring that charge carrier separation takes place efficiently. The potential drop ($\Delta\Phi_0$) within the tube wall was shown to follow the following relation:[11,22]

$$\Delta\phi_0 = \frac{kTr_0^2}{6eL_D^2} \quad (6)$$

where r_0 is half the width of the wall, T is the temperature, and L_D is the Debye length given by[11,22]

$$L_D = \left[\frac{\varepsilon\varepsilon_0 kT}{2e^2 N_D}\right]^2 \quad (7)$$

where N_D is the number of ionized donors per cm^3.[11] It is important to note that this potential drop across the wall thickness may not be enough to separate the photogenerated electrons and holes. However, because of the nanoscale dimensions of the walls (17 ± 2 nm), the holes can easily diffuse into the surface, which was shown to take place on a scale of picoseconds.[53,54] It was also reported that minority carriers generated within a distance from the surface equal to the sum of the depletion layer width and the diffusion length (retrieval length) escape recombination and reach the electrolyte.[22] Note that the relevant dimensional features of our Ti−Pd nanotube arrays (half the wall thickness) are still smaller than 10 nm, which is the value reported for crystalline TiO_2 retrieval length.[55] Therefore, bulk recombination is expected to be reduced, and the photoconversion efficiency is expected to be enhanced.[56] This is in agreement with van de Lagemaat and co-workers[56] and Allam and co-workers[22] who observed a substantial enhancement of the quantum yield in porous SiC and Ti−Nb−Zr nanotubes, respectively.

CONCLUSIONS

Vertically oriented Ti−Pd nanotube arrays were fabricated *via* anodization of Ti−Pd alloy in formamide electrolytes containing NH_4F and H_3PO_4 at room temperature. Anodization for 5 h resulted in the formation of porous structures with diameters in the range of 45 ± 5 nm. Increasing the anodization time to 15 and 24 h resulted in the formation of vertically oriented nanotube arrays ~3 and 6 μm long, respectively, with similar outer diameters of 130 ± 4 nm and wall thicknesses of 17 ± 2 nm. Annealing the as-fabricated nanotube arrays in NH_3 atmosphere at 500 °C resulted in nitrogen doping of the electrodes. Oxynitride formation was observed upon annealing the material at 550 °C for 5 h as confirmed by XPS analysis. The formation of oxynitride showed a profound effect on the visible light absorption capability of the material shifting the absorption edge to 577 nm. The 6 μm long Ti−Pd oxynitride nanotube arrays showed a three-electrode photoconversion efficiency of 0.83% (AM 1.5G illumination 100 mW/cm^2, 1.0 M KOH) when used as photoanodes to photoelectrochemically split water. This efficiency is almost 5 times higher than that obtained for pure TiO_2 nanotubes of comparable length. This enhancement in the photoconversion efficiency can be related to the synergistic effects of Pd and nitrogen doping as well as to the unique structural properties of the fabricated nanotube arrays. The obtained efficiency herein is the highest reported value so far for TiO_2 nanotube-based photoelectrochemical cell. Further extended studies are currently being done in our laboratory to investigate more combinations for efficient water photolysis.

MATERIALS AND METHODS

A two-step process was used to fabricate the Ti−Pd mixed oxynitride nanotube arrays. The arrays were first prepared by anodization of Ti−Pd alloy foil followed by annealing the amorphous Ti−Pd nanotubes in an ammonia atmosphere. Prior to anodization, Ti−0.25% Pd samples (1.5 cm × 1.0 cm × 1.0 mm) were ultrasonically cleaned with acetone, followed by a deionized water rinse. The anodization was performed in a two-electrode electrochemical cell with the titanium alloy as the working electrode and platinum foil as the counter electrode. The experiment was conducted at room temperature (approximately 22 °C) in formamide-based electrolytes containing 0.2 M NH_4F, 0.1 M H_3PO_4,

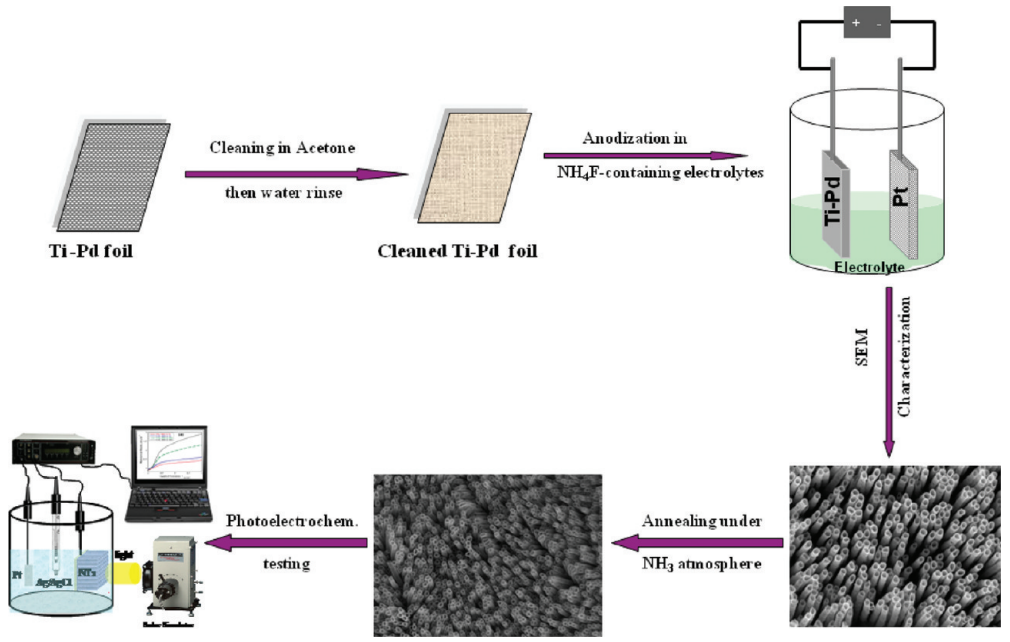

Scheme 1. Steps taken for the fabrication and testing of the Ti−Pd mixed oxynitride nanotube arrays.

and 3 vol % H_2O at 20 V for 5−24 h. An Agilent E3612A power supply was used for potentiostatic anodization. After anodization, the samples were rinsed thoroughly with deionized water and then dried under a stream of nitrogen. The as-anodized samples were annealed in an NH_3 atmosphere for 5 h at different temperatures and then left to cool under the NH_3 flow. The morphology of the samples was examined using a Zeiss Ultra60 field emission scanning electron microscope (FESEM). X-ray photoelectron spectroscopy (XPS) experiments were performed on the nanotubular films using a Thermo Scientific K-alpha XPS with an Al anode. Spectra were charge referenced to O 1s at 532 eV. The UV−vis absorption spectral measurements were performed using a Shimadzu UV−vis−NIR spectrophotometer with solid-sample holder for reflectance measurements and an integrating sphere. Photoelectrochemical properties were investigated in 1.0 M KOH solution using a three-electrode configuration with nanotube arrays as photoanodes, saturated Ag/AgCl as a reference electrode, and platinum foil as a counter electrode. A scanning potentiostat (CH Instruments, model CH 660D) was used to measure dark and illuminated currents at a scan rate of 10 mV/s. Sunlight was simulated with a 300 W xenon ozone-free lamp (Spectra Physics) and AM 1.5G filter (New Port #81094) at 100 mW/cm^2. Scheme 1 summaries the steps performed to fabricate and test the material.

Acknowledgment. We would like to thank the Department of Energy (Grant No. DE-FG02-97ER14799) and the RAK-CAM Foundation for the support of this work.

Supporting Information Available: FESEM images for Ti−Pd alloy sample anodized in formamide-based electrolyte at 20 V for 30 h, XPS N 1s spectra for samples annealed in NH_3 atmosphere at 400 and 500 °C, and the DRS UV−vis spectra of the fabricated nanotube arrays. This material is available free of charge *via* the Internet at http://pubs.acs.org.

REFERENCES AND NOTES

1. Garcia-Martinez, J.; Moniz, E. J. *Nanotechnology for the Energy Challenge*; Wiley-VCH: Weinheim, Germany, 2010.
2. Grätzel, M. Solar Energy Conversion by Dye-Sensitized Photovoltaic Cells. *Inorg. Chem.* **2005**, *44*, 6841–6851.
3. Rodríguez, J. A.; García, M. F. *Synthesis, Properties, and Applications of Oxide Nanomaterials*; John Wiley & Sons, Inc.: New York, 2007.
4. Allam, N. K.; Grimes, C. A. Room Temperature One-Step Polyol Synthesis of Anatase TiO_2 Nanotube Arrays: Photoelectrochemical Properties. *Langmuir* **2009**, *25*, 7234–7240.
5. Allam, N. K.; Grimes, C. A. Electrochemical Fabrication of Complex Copper Oxide Nanoarchitectures *via* Copper Anodization in Aqueous and Non-aqueous Electrolytes. *Mater. Lett.* **2011**, *65*, 1949–1955.
6. Allam, N. K.; Feng, X. J.; Grimes, C. A. Self-Assembled Fabrication of Vertically Oriented Ta_2O_5 Nanotube Arrays, and Membranes Thereof, by One-Step Tantalum Anodization. *Chem. Mater.* **2008**, *20*, 6477–6481.
7. Hesabi, Z. R.; Allam, N. K.; Dahmen, K.; Garmestani, H.; El-Sayed, M. A. Self-Standing Crystalline TiO_2 Nanotubes/CNTs Heterojunction Membrane: Synthesis and Characterization. *ACS Appl. Mater. Interfaces* **2011**, *3*, 952–955.
8. Allam, N. K.; Grimes, C. A. Formation of Vertically Oriented TiO_2 Nanotube Arrays Using a Fluoride Free HCl Aqueous Electrolyte. *J. Phys. Chem. C* **2007**, *111*, 13028–13032.
9. Grimes, C. A.; Mor, G. K. *TiO_2 Nanotube Arrays: Synthesis, Properties, and Applications*; Springer: Berlin, 2009.
10. Allam, N. K.; El-Sayed, M. A. Photoelectrochemical Water Oxidation Characteristics of Anodically Fabricated TiO_2 Nanotube Arrays: Structural and Optical Properties. *J. Phys. Chem. C* **2010**, *114*, 12024–12029.
11. Grimes, C. A.; Varghese, O. K.; Ranjan, S. *Light, Water, Hydrogen: The Solar Production of Hydrogen by Water Photoelectrolysis*; Springer: Norwell, MA, 2007.
12. Murphy, A. B. Does Carbon Doping of TiO_2 Allow Water Splitting in Visible Light? *Sol. Energy Mater. Sol. Cells* **2008**, *92*, 363–367.
13. Herranz, T.; Deng, X.; Cabot, A.; Alivisatos, A. P.; Liu, Z.; Soler-Illia, G.; Salmeron, M. Reactivity of Au Nanoparticles Supported Over SiO_2 and TiO_2 Studied by Ambient Pressure Photoelectron Spectroscopy. *Catal. Today* **2009**, *143*, 158–166.
14. Christopher, P.; Ingram, D. B.; Linic, S. Enhancing Photochemical Activity of Semiconductor Nanoparticles with Optically Active Ag Nanostructures: Photochemistry Mediated by Ag Surface Plasmons. *J. Phys. Chem. C* **2010**, *114*, 9173–9177.
15. Rettew, R. E.; Allam, N. K.; Alamgir, F. M. Interface Architecture Determined Electrocatalytic Activity of Pt on Vertically Oriented TiO_2 Nanotubes. *ACS Appl. Mater. Interfaces* **2011**, *3*, 147–151.

16. Hayden, S. C.; Allam, N. K.; El-Sayed, M. A. TiO_2 Nanotube/CdS Hybrid Electrodes: Extraordinary Enhancement in the Inactivation of *Escherichia coli*. *J. Am. Chem. Soc.* **2010**, *132*, 14406–14408.
17. Galoppini, E. Linkers for Anchoring Sensitizers to Semiconductor Nanoparticles. *Coord. Chem. Rev.* **2004**, *248*, 1283–1297.
18. Oyama, M.; Orimo, A.; Nouneh, K. Effects of Linker Molecules on the Attachment and Growth of Gold Nanoparticles on Indium Tin Oxide Surfaces. *Electrochim. Acta* **2009**, *54*, 5042–5047.
19. Mor, G. K.; Prakasam, H. E.; Varghese, O. K.; Shankar, K.; Grimes, C. A. Vertically Oriented Ti−Fe−O Nanotube Array Films: Toward a Useful Material Architecture for Solar Spectrum Water Photoelectrolysis. *Nano Lett.* **2007**, *7*, 2356–2364.
20. Mor, G. K.; Varghese, O. K.; Wilke, R. H. T.; Sharma, S.; Shankar, K.; Latempa, T. J.; Choi, K. S.; Grimes, C. A. p-Type Cu−Ti−O Nanotube Arrays and Their Use in Self-Biased Heterojunction Photoelectrochemical Diodes for Hydrogen Generation. *Nano Lett.* **2008**, *8*, 1906–1911.
21. Kusama, H.; Wang, N.; Miseki, Y.; Sayama, K. Combinatorial Search for Iron/Titanium-Based Ternary Oxides with a Visible-Light Response. *J. Comb. Chem.* **2010**, *12*, 356–362.
22. Allam, N. K.; Alamgir, F.; El-Sayed, M. A. Enhanced Photo-assisted Water Electrolysis Using Vertically Oriented Anodically Fabricated Ti−Nb−Zr−O Mixed Oxide Nanotube Arrays. *ACS Nano* **2010**, *4*, 5819–5826.
23. Yamasita, D.; Takata, T.; Hara, M.; Kondo, J. N.; Domen, K. Recent Progress of Visible-Light-Driven Heterogeneous Photocatalysts for Overall Water Splitting. *Solid State Ionics* **2004**, *172*, 591–595.
24. Vitiello, R. P.; Macak, J. M.; Ghicov, A.; Tsuchiya, H.; Dick, L. F. P.; Schmuki, P. N-Doping of Anodic TiO_2 Nanotubes Using Heat Treatment in Ammonia. *Electrochem. Commun.* **2006**, *8*, 544–548.
25. Martinez-Ferrero, E.; Sakatani, Y.; Boissière, C.; Grosso, D.; Fuertes, A.; Fraxedas, J.; Sanchez, C. Nanostructured Titanium Oxynitride Porous Thin Films as Efficient Visible-Active Photocatalysts. *Adv. Funct. Mater.* **2007**, *17*, 3348–3354.
26. Kim, D.; Fujimoto, S.; Schmuki, P.; Tsuchiya, H. Nitrogen Doped Anodic TiO_2 Nanotubes Grown from Nitrogen-Containing Ti Alloys. *Electrochem. Commun.* **2008**, *10*, 910–913.
27. Hitoki, G.; Takata, T.; Kondo, J. N.; Hara, M.; Kobayashi, H.; Domen, K. (Oxy)Nitrides as New Photocatalysts for Water Splitting under Visible Light Irradiation. *Electrochemistry* **2002**, *70*, 463–465.
28. Li, Q.; Liang, W.; Shang, J. K. Enhanced Visible-Light Absorption from PdO Nanoparticles in Nitrogen-Doped Titanium Oxide Thin Films. *Appl. Phys. Lett.* **2007**, *90*, 063109.
29. Li, Q.; Xie, R.; Mintz, E. A.; Shang, J. K. Effect of Precursor Ratio on Synthesis and Optical Absorption of TiON Photocatalytic Nanoparticles. *J. Am. Ceram. Soc.* **2007**, *90*, 3863–3868.
30. Hsiao, Y.-C.; Tseng, Y.-H. Preparation of Pd-Containing TiO_2 Film and Its Photocatalytic Properties. *Micro Nano Lett.* **2010**, *5*, 317–320.
31. Su, H.; Dong, Q.; Han, J.; Zhang, D.; Guo, Q. Biogenic Synthesis and Photocatalysis of Pd−PdO Nanoclusters Reinforced Hierarchical TiO_2 Films with Interwoven and Tubular Conformations. *Biomacromolecules* **2008**, *9*, 499–504.
32. Lee, S.-K.; Mills, A. Platinum and Palladium in Semiconductor Photocatalytic Systems. *Platinum Met. Rev.* **2003**, *47*, 61–72.
33. Meyer, S.; Saborowski, S.; Schäfer, B. Photocatalytic Reforming of Methanol by Spatially Separated Pd Particles on Special TiO_2 Layers. *ChemPhysChem* **2006**, *7*, 572–574.
34. Hass, K. C.; Carlsson, A. E. Band Strucyures of Nonmagnetic Transition-Metal Oxides—PdO and PtO. *Phys. Rev. B* **1992**, *46*, 4246–4249.
35. Pilloy, T.; Zimmermann, R.; Steiner, P.; Hufner, S. The Electronic Structure of PdO Found by Photoemission (UPS and XPS) and Inverse Photoemission (BIS). *J. Phys.: Condens. Matter.* **1997**, *9*, 3987–3999.
36. Allam, N. K.; Shankar, K.; Grimes, C. A. A General Method for the Anodic Formation of Crystalline Metal Oxide Nanotube Arrays without the Use of Thermal Annealing. *Adv. Mater.* **2008**, *20*, 3942–3946.
37. Allam, N. K.; Grimes, C. A. Effect of Rapid Infrared Annealing on the Photoelectrochemical Properties of Anodically Fabricated TiO_2 Nanotube Arrays. *J. Phys. Chem. C* **2009**, *113*, 7996–7999.
38. Kuroda, Y.; Mori, T.; Yagi, K.; Makihata, N.; Kawahara, Y.; Nango, M.; Kittaka, S. Preparation of Visible-Light-Responsive $TiO_{2-x}N_x$ Photocatalyst by a Sol−Gel Method: Analysis of the Active Center on TiO_2 that Reacts with NH_3. *Langmuir* **2005**, *21*, 8026–8034.
39. Yang, X.; Li, C.; Yang, B.; Wang, W.; Qiam, Y. Optical Properties of Titanium Oxynitride Nanocrystals Synthesized *via* a Thermal Liquid−Solid Metathesis Reaction. *Chem. Phys. Lett.* **2004**, *383*, 502–506.
40. Chan, M. H.; Lu, F. H. X-ray Photoelectron Spectroscopy Analyses of Titanium Oxynitride Films Prepared by Magnetron Sputtering Using Air/Ar Mixtures. *Thin Solid Films* **2009**, *517*, 5006–5009.
41. Varghese, O. K.; Paulose, M.; LaTempa, T. J.; Grimes, C. A. High-Rate Solar Photocatalytic Conversion of CO_2 and Water Vapor to Hydrocarbon Fuels. *Nano Lett.* **2009**, *9*, 731–737.
42. Braic, M.; Balaceanu, M.; Vladescu, A.; Kiss, A.; Braic, V.; Epurescu, G. Preparation and Characterization of Titanium Oxy-Nitride Thin Films. *Appl. Surf. Sci.* **2007**, *253*, 8210–8214.
43. Briggs, D.; Gran, T. J. *Surface Analysis by Auger and X-ray Photoelectron Spectroscopy*; IM Publications: Chichester, UK, 2003.
44. Strydom, I. R.; Hofmann, S. The Contribution of Characteristic Energy-Loss in the Core-Level X-ray Photoelectron Spectroscopy Peaks of Tin and (Ti,Al)N Studied by Electron Energy-Loss Spectroscopy and X-ray Photoelectron Spectroscopy. *J. Electron Spectrosc. Relat. Phenom.* **1991**, *56*, 85–103.
45. Mi, L.; Xu, P.; Wang, P. N. Experimental Study on the Bandgap Narrowings of TiO_2 Films Calcined under N_2 or NH_3 Atmosphere. *Appl. Surf. Sci.* **2008**, *255*, 2574–2580.
46. Asahi, R.; Morikawa, T.; Ohwaki, T.; Aoki, K.; Taga, Y. Visible-Light Photocatalysis in Nitrogen-Doped Titanium Oxides. *Science* **2001**, *293*, 269–271.
47. Saha, N. C.; Tompkins, H. G. Titanium Nitride Oxidation Chemistry: An X-ray Photoelectron Spectroscopy Study. *J. Appl. Phys.* **1992**, *72*, 3072–3079.
48. Wu, Z.; Sheng, Z.; Liu, Y.; Wang, H.; Tang, N.; Wang, J. Characterization and Activity of Pd-Modified TiO_2 Catalysts for Photocatalytic Oxidation of NO in Gas Phase. *J. Hazard. Mater.* **2009**, *164*, 542–548.
49. Kosowska, B.; Mozia, S.; Morawski, A. W.; Grzmil, B.; Janus, M.; Kalucki, K. The Preparation of TiO_2-Nitrogen Doped by Calcination of $TiO_2 \cdot xH_2O$ under Ammonia Atmosphere for Visible Light Photocatalysis. *Sol. Energy Mater. Sol. Cells* **2005**, *88*, 269–280.
50. Gartner, M.; Osiceanu, P.; Anastasescu, M.; Stoica, T.; Trapalis, C.; Giannakopoulou, T.; Todorova, N.; Lagoyannis, A. Investigation on the Nitrogen Doping of Multilayered, Porous TiO_2 Thin Films. *Thin Solid Films* **2008**, *516*, 8184–8189.
51. Sieradzka, K.; Kaczmarek, D.; Domaradzki, J.; Prociów, E.; Mazur, M.; Górnicka, B. Optical and Electrical Properties of Nanocrystalline TiO_2:Pd Semiconducting Oxides. *Cent. Eur. J. Phys.* **2011**, *9*, 313–318.
52. Ruan, C. M.; Paulose, M.; Varghese, O. K.; Mor, G. K.; Grimes, C. A. Fabrication of Highly Ordered TiO_2 Nanotube Arrays Using an Organic Electrolyte. *J. Phys. Chem. B* **2005**, *109*, 15754–15759.
53. Hagfeldt, A.; Gratzel, M. Light-Induced Redox Reactions in Nanocrystalline Systems. *Chem. Rev.* **1995**, *95*, 49–68.

54. Vanmaekelbergh, D.; de Jongh, P. E. Driving Force for Electron Transport in Porous Nanostructured Photoelectrodes. *J. Phys. Chem. B* **1999**, *103*, 747–750.
55. Sukamto, J. P. H.; Smyrl, W. H.; Mcmillan, C. S.; Kozlowski, M. R. Photoelectrochemical Measurements of Thin Oxide-Films: Multiple Iinternal-Reflection Effects. *J. Electrochem. Soc.* **1992**, *139*, 1033–1043.
56. van de Lagemaat, J.; Plakman, M.; Vanmaekelbergh, D.; Kelly, J. J. Enhancement of the Light-to-Current Conversion Efficiency in an n-SiC/Solution Diode by Porous Etching. *Appl. Phys. Lett.* **1996**, *69*, 2246–2248.